

# A classification based on tumor budding and immune score for patients with hepatocellular carcinoma

Li Wei<sup>a\*</sup>, Zhang Delin<sup>a\*</sup>, Yuan Kefe<sup>a</sup>, Wu Hong<sup>a</sup>, Huang Jiwei<sup>a</sup>, and Zhang Yange<sup>b</sup>

<sup>a</sup>Department of Liver Surgery & Liver Transplantation, State Key Laboratory of Biotherapy and Cancer Center, West China Hospital, Sichuan University and Collaborative Innovation Center of Biotherapy, Chengdu, China; <sup>b</sup>Department of Plastic and Burns Surgery, West China Hospital, Sichuan University, Chengdu, China

## ABSTRACT

**Background:** The role of immune profiling and tumor budding in hepatocellular carcinoma (HCC) remains largely unknown. This study evaluated the association between tumor budding and lymphocytic infiltration in HCC. Meanwhile, HCC patients were stratified based on tumor budding grade and immune score.

**Patients and methods:** A total of 423 HCC patients were divided into training (n = 212) and validation (n = 211) cohort. Tumor slides from resected HCC samples were used for tumor budding assessment. A prognosis-relevant immune score was developed based on five types of immune cells out of eleven immune markers. A classification based on tumor budding grade and immune type was established (IS-TB type). To explore the association of IS-TB type and molecular alterations of HCC, 100 HCC samples and adjacent non-tumor tissues from 100 patients were investigated by whole-exome sequencing.

**Results:** Tumor budding was an independent adverse prognostic factor for OS and DFS in both of the training and validation cohorts (all *P* values <.05). The rate of high-grade tumor budding was significantly higher in HCC with immature stroma (*P* <.001), strong  $\alpha$ -SMA expression (*P* = .005), non-steatotic tumors and non-fibrolamellar-HCC (*P* <.001). Additionally, tumor budding was related to both anti- and pro-tumor immune responses. Patients were classified into immune type A and immune type B according to the immune score. Based on tumor budding grade and immunotype, patients were classified into four subgroups: IS<sub>A</sub>-TB<sub>high</sub> (type I), IS<sub>B</sub>-TB<sub>high</sub> (type II), IS<sub>A</sub>-TB<sub>low</sub> (type III) and IS<sub>B</sub>-TB<sub>low</sub> (type IV). Patients with type III tumor had the best OS and DFS, whereas OS and DFS were the worst for cases with type II tumor. TP53 mutation was more frequent in IS-TB type I (IS<sub>A</sub>TB<sub>high</sub>) patients, while IS-TB type IV (IS<sub>B</sub>TB<sub>low</sub>) harbored high number of CTNNB1 mutation.

**Conclusion:** Tumor-immune cell interactions in HCC is heterogeneous. HCC classification based on tumor budding and immune score correlates with patient survival and molecular alterations. The defined subtypes may have significance for utilizing individualized treatment in patients with HCC.

## ARTICLE HISTORY

Received 1 May 2019  
Revised 18 September 2019  
Accepted 21 September 2019

## KEYWORDS

Hepatocellular carcinoma; tumor budding; immune score; prognosis; whole exome sequencing



## Background

Liver cancer is the fifth most common cancer and the second most lethal cancer globally.<sup>1</sup> The most common type of liver cancer is hepatocellular carcinoma (HCC). Currently, the tumor-node-metastasis (TNM) system is still the gold standard for risk stratification of HCC patients for current management regimes.<sup>2</sup> However, recurrence and survival for patients with HCC vary widely within each stage grouping.<sup>3–5</sup> In addition to the TNM staging, some histologic subtypes based on the World Health Organization classification has classified patients into distinguishing prognostic subgroups. However, the prognostic value of the histologic types such as tumor grade (differentiation) still remains unsatisfactory.<sup>6</sup> In HCC, other alternative grading system or histologic features should be established or identified for estimation of patient outcome and therewith therapeutic patient stratification.


Tumor budding, first introduced in colorectal tumors, was defined as the presence of single tumor cell or small groups of

up to four tumor cells at the intratumoral area or invasive front.<sup>7–11</sup> In colorectal cancer, the Union of International Cancer Control classified tumor budding as an “additional prognostic indicator”.<sup>12</sup> In addition to colorectal cancers, tumor budding is also a novel prognostic indicator independent of tumor stage and tumor grade in diverse types of tumor including esophageal, gastric, bladder, lung and pancreatic tumors.<sup>11,13–19</sup> However, the prognostic value of tumor budding in HCC remains unknown. Tumor budding is thought to be a reflection of epithelial–mesenchymal transition (EMT) process and it is featured by two malignant characteristics, cellular discohesion, and active invasion.<sup>20,21</sup> In addition, tumor budding phenotype showed constitutive activation of the WNT signaling pathway, and the downstream molecule  $\beta$ -catenin was deemed as integral components of EMT process.<sup>22</sup>

In addition, tumor-infiltrating lymphocytes (TILs) significantly correlate with patient outcome in multiple types of

**CONTACT** Zhang Yange  58131972@qq.com  Department of Plastic and Burns Surgery, West China Hospital, Sichuan University, Chengdu 610041, China

\*Co-first author.

 Supplemental data for this article can be accessed on the [publisher's website](#).

© 2019 The Author(s). Published with license by Taylor & Francis Group, LLC.

This is an Open Access article distributed under the terms of the Creative Commons Attribution-NonCommercial License (<http://creativecommons.org/licenses/by-nc/4.0/>), which permits unrestricted non-commercial use, distribution, and reproduction in any medium, provided the original work is properly cited.

cancer including HCC.<sup>23-28</sup> For example, in HCC, the pioneering studies demonstrated that CD8+ and CD45RO+ T-cell infiltration were independent favorable prognostic factors indicating patient survival.<sup>29,30</sup> The tumor microenvironment (TME) is crucial for the local progression of tumor cells, since specific immune profiles may lead to the TME permissible for single tumor cell invasion (tumor budding).<sup>31</sup> However, previous studies usually reported tumor budding and tumor-immune phenotype independently.<sup>19,32</sup> A detailed characterization of the TME integrating tumor- and host-associated indicators may lead to the identification of novel prognosis-relevant factors and pathways. Thus, in the present study, we illustrated the prognostic role of tumor budding in HCC and investigated whether tumor budding associated with tumor-infiltrating lymphocytes. Additionally, we classified HCC patients into four subgroups based on tumor budding and immune score.

## Patients and methods

### Patient cohort and pathological examination

Four hundred and twenty-three HCC patients were entered into this study. Details of patient identification from the total cohort are shown in the supplementary materials. Patients were treated by radical surgical resection at the West China Hospital, Sichuan University between January 2009 and December 2017. The details of study design and flow chart are shown in Figure 1. Informed consent was obtained from all patients. This study was also approved by the review board

committee of the West China Hospital. The surgical procedure was performed as in our previous study.<sup>33</sup> Patients were randomly divided into training cohort (n = 212) and validation cohort (n = 211). Details regarding patient follow-up after surgery are presented in the supplementary materials.

Tumor staging was carried out based on the Barcelona Clinic Liver Cancer (BCLC) system and TNM staging system (eighth). The Albumin-Bilirubin (ALBI) grade was used to assess preoperative liver function in HCC cases.<sup>34</sup> The histological subtypes and grades were determined according to the WHO classification by two pathologists (Li W and Yuan KF). The following pathological features were classified and defined: grades of steatosis (Grade 0: absent or minimal, Grade 1: <30%, Grade 2: 30–60%, Grade 3: >60%); tumor differentiation (Grade I-IV: according to Edmondson-Steiner grade); Pseudoglandular histological pattern (presence of a pseudoglandular pattern, as defined by the World Health Organization, in at least 20% of the tumor); Trabecular histological pattern (presence of a trabecular pattern, as defined by the World Health Organization, in at least 20% of the tumor); fibrolamellar-HCC (cirrhotic subtype of HCC, as defined by the World Health Organization). The stromal maturity was defined based on previous literature.<sup>35</sup>

### Tumor budding evaluation

Tumor budding was classified into Grade 1 (0–4), Grade 2 (5–9) and Grade 3 ( $\geq 10$ ). In addition, cases with  $\geq 10$  buds were defined as high-grade tumor budding, those with 0 to 9

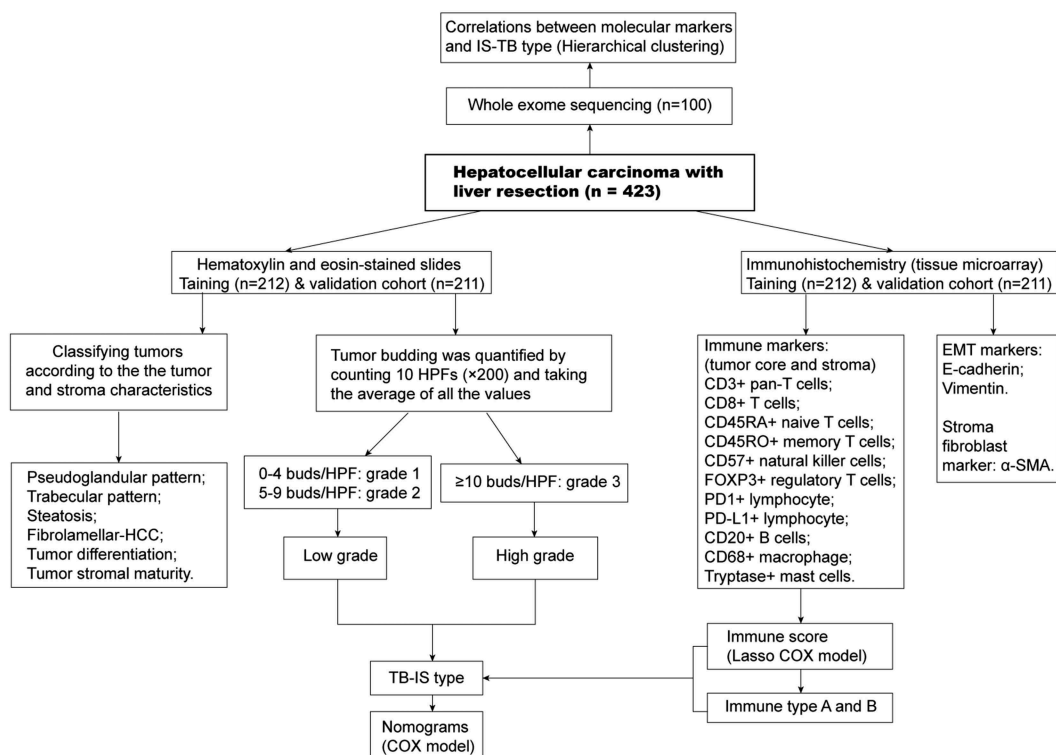


**Figure 1.** Flowchart of the study design. Tumor budding was graded into grade 1 (0–4), grade 2 (5–9) and grade 3 ( $\geq 10$ ). In addition, cases with  $\geq 10$  buds were classified as high-grade tumor budding, those with 0 to 9 buds were classified as low-grade tumor budding. HCC-specific pathological patterns were also confirmed in Hematoxylin-eosin-stained slides. Eleven immune biomarkers were stained by immunohistochemistry. Moreover,  $\alpha$ -SMA and EMT markers including E-cadherin and vimentin were stained. Whole exome sequencing was performed in one hundred pairs of tumoral and non-tumoral samples.

buds were defined as low-grade tumor budding.<sup>19,36</sup> Tumor budding has been evaluated according to the International Tumor Budding Consensus Conference (ITBCC) method.<sup>11</sup> Two experienced pathologists (Li W and Yuan KF) independently searched all slides throughout at low magnification. We selected the “hotspot” area method (which is considered to be the most useful method for evaluating tumor budding in colorectal tumor) to estimate the number of tumor budding. Tumor buds in this area (intratumoral or at the invasive front) were counted at 20x magnification (field area 0.785 mm<sup>2</sup>). The inter-observer agreement was evaluated by the intra-class correlation coefficient for the number of buds and Kappa statistic ( $\kappa$ ) for categorical counts. An example of tumor budding is shown in Figure S1.

### **Immunohistochemistry and hematoxylin-eosin staining**

Hematoxylin-eosin (HE) and Immunohistochemistry (IHC) staining were done as described in Supplementary methods. Based on findings of previous studies,<sup>32,37,38</sup> 11 types of immune biomarkers were selected for IHC staining: pan T cells (CD3), B cells (CD20), memory T cells (CD45RO), cytotoxic T cells (CD8), naive T cells (CD45RA), natural killer cells (CD57), mast cells (tryptase), macrophages (CD68), regulatory T cells (FOXP3), PD1+ immune cells and PD-L1+ immune cells. In addition, we used  $\alpha$ -SMA, a fibroblast activation marker, to represent fibrotic stroma activity. EMT markers including E-cadherin and vimentin were stained. The details of the primary antibodies for IHC staining are shown in Table S1. The procedural of cell quantitation are shown in the Supplementary materials.

### **Whole exome sequencing**

After extraction of genomic tumoral and non-tumoral DNA from frozen samples using a Promega Maxwell® Instrument with the Maxwell® 16 System DNA Purification Kit. DNA was quantitated using Hoechst dyes and a microplate reader. The detailed process for enrichment of individual genomic DNA (gDNA) sample libraries is shown in Supplementary materials (using SureSelect XT Target Enrichment System). After qualifying libraries of tumor and non-tumor tissues, they were sequenced by SureSelectXT Human All Exon V6 (target size 60 Mb, Agilent, Santa Clara, CA) and paired-end sequencing was carried out on a Illumina HiSeq X Ten, PE150 with 2 × 150 base pairs (bp) read length. Raw data and base calls were processed using standard Illumina Miseq Reporter software (version 2.5.1). The downstream data analysis was done on the resulting Illumina FASTQ files. The reads were aligned on human hg19 genome reference utilizing BWA version 0.7.5a and bam files were generated using samtools v1.3.

### **Statistical analysis**

Categorical variables are shown as number (%) and tested by Chi-square test or Fisher’s exact test. Continuous variables are shown as mean  $\pm$  SD and examined by t-test or Kruskal–Wallis test. The time of disease-free survival (DFS) was calculated from the date of hepatectomy to the date of the first recurrence,

death or the last follow-up. Overall survival (OS) was defined as the time from liver resection to the last follow-up (January 1, 2019) or death. The survival data were compared by the log-rank test.

Immune cells in tumor stroma were more prognosis-relevant than immune cells in tumor core (data not shown), thus immune cell count in the stroma was utilized to build the immune score. We utilized the LASSO COX model to identify the most significant prognostic parameters out of 11 features for lymphocytes (CD3, CD20, CD8, CD45RO, CD45RA, CD57, CD68, FOXP3, Tryptase, PD1 and PD-L1), and then constructed a classifier according to multiple immune parameters for predicting DFS in the training cohort. The R package “glmnet” was selected to carry out the LASSO COX analyses. The interaction test was used to examine the influence of each stratified factor on the relationship between immune score and patient prognosis. Besides, two nomograms integrating clinical parameters and immune type were constructed based on outcomes from the multivariate COX analyses. We adjusted for variables which changed HR or  $\beta$  more than 10% when they were removed from or added to the models.<sup>39</sup> In addition, we also adjusted clinically clear prognostic indicators which did not meet this condition. Covariates included in the COX models were sex, age, HBV infection, HBV-DNA level, alpha fetoprotein (AFP) level, BCLC stage, ALBI grade, microvascular invasion (MVI), tumor differentiation, and tumor budding and immune score type. Calibration plots were also constructed to determine the performance features of the models. The discriminative abilities of the models were evaluated by the receiver operating characteristic curve (AUC). Harrell index of concordance (C-index) was also calculated to compare the accuracy of the predictive models. All statistical analysis was carried out by R 3.4.3 (<http://www.R-project.org>).

## **Results**

### **Patient characteristics and pathological examination**

The clinicopathologic features of HCC patients in the two cohorts are shown in Table 1. There was a male predominance (83.5%), with main risk factor being hepatitis B virus infection (85.6%). High AFP levels ( $\geq 400$  ng/ml) were found in 39.2% of the cases. The mean tumor size was 6.1  $\pm$  3.7 (mean  $\pm$  SD) cm and 78.3% of patients had single tumors. Distinct tumor stages were included with early (BCLC A, 79.2%) as well as intermediate (BCLC B, 20.8%) tumors.

There were 285 (67.7%) and 136 (32.3%) cases of well (Edmondson grade I-II) and poorly (Edmondson grade III-IV) differentiated tumors, respectively. Areas with thin, moderate and thick trabecular histological architectural patterns were identified in 33 (7.8%), 64 (15.1%) and 77 (18.2%) of the tumors. Pseudoglandular and fibrolamellar-HCC were observed in 61 (14.4%) and 27 (6.4%) of tumors. Grade 1, 2 and 3 steatosis were found in 68 (16.1%), 47 (11.1%) and 82 (19.4%) of tumors. Finally, grade 1, 2 and 3 tumor budding were identified in 160 (37.8%), 111 (26.2%) and 152 (35.9%) patients, respectively. Baseline clinicopathologic characteristics

**Table 1.** Clinicopathologic characteristics of patients.

Variable	Total cohort (n = 423)	Training cohort (n = 212)	Validation cohort (n = 211)	P-value*
Age, years	51.0 ± 12.2	51.0 ± 11.9	51.0 ± 12.6	0.959
Gender				0.198
Male	353 (83.5%)	172 (81.1%)	181 (85.8%)	
Female	70 (16.5%)	40 (18.9%)	30 (14.2%)	
HBV infection				0.323
Negative	61 (14.4%)	27 (12.7%)	34 (16.1%)	
Positive	362 (85.6%)	185 (87.3%)	177 (83.9%)	
AFP, ng/mL				0.152
<400	257 (60.8%)	136 (64.2%)	121 (57.3%)	
≥400	166 (39.2%)	76 (35.8%)	90 (42.7%)	
Tumor size, cm	6.1 ± 3.7	6.0 ± 3.6	6.2 ± 3.8	0.736
Tumor number				0.464
Single	331 (78.3%)	169 (79.7%)	162 (76.8%)	
Multiple	92 (21.7%)	43 (20.3%)	49 (23.2%)	
ALBI score	-2.8 ± 0.4	-2.8 ± 0.4	-2.8 ± 0.3	0.934
AJCC-TNM Stage				0.674
Stage I	238 (56.3%)	120 (56.6%)	118 (55.9%)	
Stage II	136 (32.2%)	65 (30.7%)	71 (33.6%)	
Stage III	49 (11.6%)	27 (12.7%)	22 (10.4%)	
BCLC Classification				0.614
A	335 (79.2%)	170 (80.2%)	165 (78.2%)	
B	88 (20.8%)	42 (19.8%)	46 (21.8%)	
MVI				0.540
No	301 (71.2%)	148 (69.8%)	153 (72.5%)	
Yes	122 (28.8%)	64 (30.2%)	58 (27.5%)	
Tumor differentiation				0.117
Grade I-II	285 (67.7%)	136 (64.2%)	149 (71.3%)	
Grade III-IV	136 (32.3%)	76 (35.8%)	60 (28.7%)	
Pseudoglandular structure				0.323
No	362 (85.6%)	185 (87.3%)	177 (83.9%)	
Yes	61 (14.4%)	27 (12.7%)	34 (16.1%)	
Trabecular structure				0.784
None	249 (58.9%)	122 (57.5%)	127 (60.2%)	
Thin	33 (7.8%)	15 (7.1%)	18 (8.5%)	
Moderate	64 (15.1%)	33 (15.6%)	31 (14.7%)	
Thick	77 (18.2%)	42 (19.8%)	35 (16.6%)	
Steatosis				0.279
None	226 (53.4%)	116 (54.7%)	110 (52.1%)	
Grade 1	68 (16.1%)	27 (12.7%)	41 (19.4%)	
Grade 2	47 (11.1%)	24 (11.3%)	23 (10.9%)	
Grade 3	82 (19.4%)	45 (21.2%)	37 (17.5%)	
Fibrolamellar-HCC				0.542
No	396 (93.6%)	200 (94.3%)	196 (92.9%)	
Yes	27 (6.4%)	12 (5.7%)	15 (7.1%)	
Tumor budding				0.283
Grade 1	160 (37.8%)	87 (41.0%)	73 (34.6%)	
Grade 2	111 (26.2%)	56 (26.4%)	55 (26.1%)	
Grade 3	152 (35.9%)	69 (32.5%)	83 (39.3%)	

HBV, hepatitis b virus; AFP, alpha fetoprotein; ALBI, albumin-bilirubin; AJCC, American Joint Committee on Cancer; BCLC, Barcelona Clinic Liver Cancer; MVI, microvascular invasion. \*, P values were generated by comparing data of the training and validation cohorts.

between training and validation cohorts showed no significant difference (Table 1).

### Tumor budding and patient survival

The representative HE images of grade 1–3 tumor budding are shown in Figure 2(a–c). In univariate analyses (Table S2 and S3), no significances in OS and DFS were observed in grade 1 and grade 2 groups, thus we integrated grade 1 and 2 tumor budding subgroups into one group (low grade). Survival analyses were performed to compare the OS and DFS between low grade and high grade (grade 3) groups. The results demonstrated that patients with low-grade tumor budding showed better OS and DFS compared to those with high-grade tumor budding in both trainings (Figure 2(d–e)) and validation (Figure 2(g–h)) cohorts. In the training cohort, the 3-year OS rate for patients with low or high tumor budding was 80.3% and 53.8%, respectively, and the 3-year DFS

rate was 67.8% and 47.4%, respectively. In the validation cohort, 3-year OS and DFS rates for cases with low-grade tumor budding were also significantly higher than they were for cases with high-grade budding (OS: 84.2% vs. 58.4%; DFS: 70.2% vs. 48.4%). After adjusting confounding factors shown in Figure 2(f,i) tumor budding was an independent prognostic indicator for both OS and DFS in training (OS: hazard ratio, 1.60; 95% CI, 1.29–1.99; DFS: hazard ratio, 1.46; 95% CI, 1.18–1.80) and validation (OS: hazard ratio, 1.64; 95% CI, 1.32–2.05; DFS: hazard ratio, 1.50; 95% CI, 1.21–1.86) cohorts.

### Tumor budding and clinicopathologic characteristics

Clinical features including age, sex, AFP level, tumor stage, background liver cirrhosis, and MVI showed no significant differences between high and low-grade tumor budding groups (Table S4). In Figure S2 and Figure 3(a), we showed the representative HE images of different pathologic patterns including



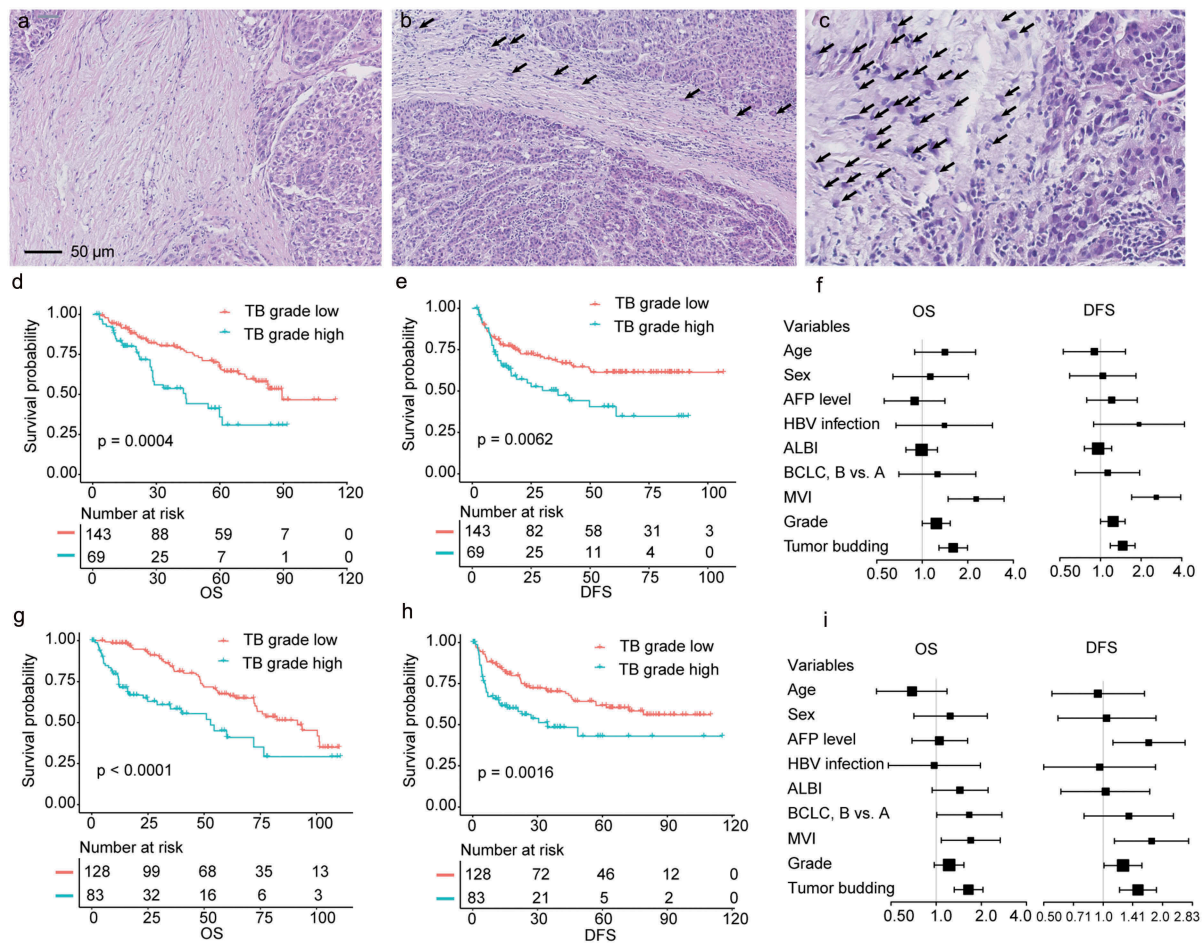


**Figure 2.** Representative images of grade 1–3 tumor budding and the prognostic role of tumor budding in training and validation cohorts. (a–c), Representative images of grade 1–3 tumor budding. (d), Survival analysis comparing overall survival (OS) between tumor budding (TB)-grade-high and TB-grade-low groups in the training cohort. (e), Disease-free survival (DFS) analyses in the training cohort. (f), the forest map showed that TB was an adverse prognostic factor for both OS and DFS in the training cohort after adjusting confounding factors. (g–h), Survival analysis comparing OS (G) and DFS (H) between tumor TB-grade-high and TB-grade-low groups in the validation cohort. (i), the forest map showed that TB was an adverse prognostic factor for both OS and DFS in the validation cohort. AFP, alpha fetoprotein; HBV, hepatitis-B virus; ALBI, albumin-bilirubin; BCLC, Barcelona Clinic Liver Cancer staging system; MVI, microvascular invasion.

tumor architectural pattern, stromal features, and EMT-related markers. As expected, high-grade tumor budding was significantly associated with high vimentin ( $P = .002$ ) and low E-cadherin ( $P = .005$ ) expressions (Figure 3(b)). Interestingly, the rate of high-grade tumor budding was significantly higher in tumors with immature stroma ( $P < .001$ ) and strong  $\alpha$ -SMA expression ( $P = .005$ ) (Figure 3(c)). In addition, high-grade tumor budding was most frequently identified in non-steatotic tumors ( $P < .001$ ) (Figure 3(d)). Fibrolamellar-HCC exhibited less frequent high-grade tumor budding than other tumors ( $P < .001$ ) (Figure 3(d)). However, tumor budding was not related to tumor differentiation ( $P = .344$ ), pseudoglandular ( $P = .954$ ) and trabecular pathologic patterns ( $P = .799$ ) (Figure 3(d)).

### Tumor budding and immune cell markers

Infiltration of most immune cell types was positively correlated (Figure S3). A heat-map graphical representation of the main immune cell infiltration linked to different tumor budding grades (grade 1–3) is provided in Figure 3(e). High-grade tumor budding was significantly correlated with high stromal

CD8+ ( $P = .002$ ), CD20+ ( $P = .009$ ), CD45RO+ ( $P = .003$ ) and CD45RA+ ( $P = .026$ ) lymphocyte infiltration (Figure 4(g)). Noticeably, high-grade tumor budding was also positively correlated with PD1+ ( $P < .001$ ) and CD68+ ( $P < .001$ ) immune cells. Whereas there was no correlation between tumor budding and tumoral CD3+ immune cell infiltration ( $P = .776$ ), tumoral CD57+ lymphocyte infiltration ( $P = .165$ ), tumoral FOXP3+ lymphocyte infiltration ( $P = .511$ ), tumoral PD-L1+ immune cell infiltration ( $P = .778$ ) and tumoral mast-cell infiltration ( $P = .939$ ) (Figure 4(m)). The representative images of the 11 types of immune cells were presented in Figure 4(a–f) and Figure 4(h–l).

### Classification of HCC based on tumor budding and immune score (IS-TB type)

LASSO COX was used to establish a prognostic score for DFS in the training group, which combined five parameters ( $CD8_{stromal}$ ,  $PD-L1_{stromal}$ ,  $Mast-cell_{stromal}$ ,  $CD68_{stromal}$ , and  $FOXP3_{stromal}$ ) out of the 11 types of immune markers (Figure S4). Utilizing the coefficients from the LASSO COX analyses, a formula was established to calculate for a single patient (Figure S4a–b). On

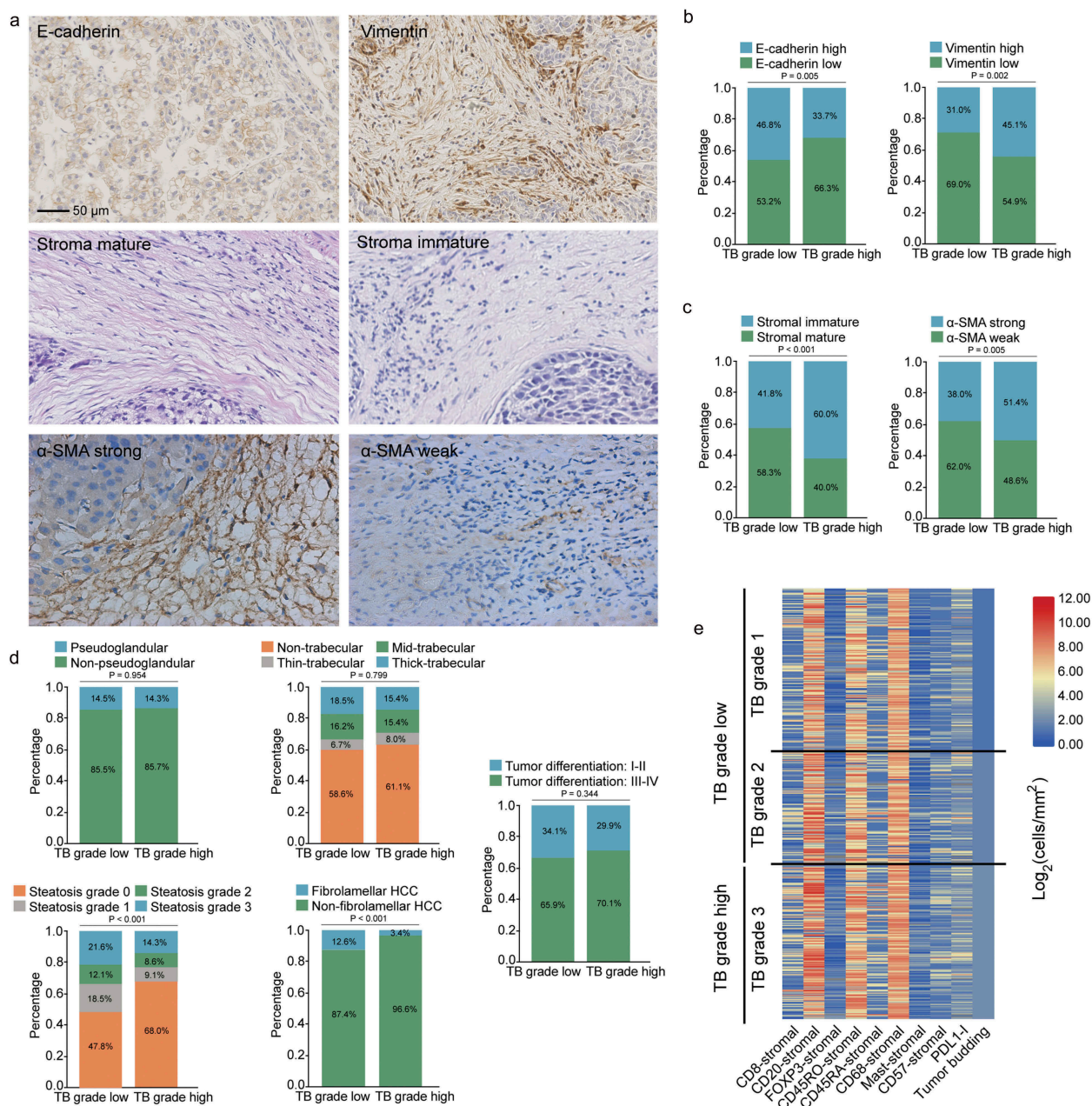


**Figure 3.** Associations of tumor budding with pathological and immune features. (a) representative images of E-cadherin, vimentin,  $\alpha$ -SMA and stromal maturity. (b) Associations of tumor budding with E-cadherin and vimentin expressions (E-cadherin and vimentin were divided into high and low groups by the median values of expression levels). (c) Associations of tumor budding with stromal features including  $\alpha$ -SMA expression and tumor maturity. (d) Associations of tumor budding with HCC pathological patterns including pseudoglandular, trabecular, steatotic, cirrhotic-HCC and tumor differentiation. (e) the heat map shows the main immune cell infiltrations linked to tumor budding grade. PDL1-I, PDL1-immune cells.

the basis of the Z-score of the personalized levels of the five parameters, the immunoscore is  $(-0.25 \times \text{CD8}_{\text{stromal}}) + (0.03 \times \text{PD-L1}_{\text{stromal}}) + (0.01 \times \text{Mast-cell}_{\text{stromal}}) + (0.21 \times \text{CD68}_{\text{stromal}}) + (0.20 \times \text{FOXP3}_{\text{stromal}})$ . With a median value of 0.04 as the cutoff value, we classified patients into immune type A and immune type B groups. As shown in Figure S4d–e and S4g–h, cases in immune type A group showed significantly better DFS and OS than those in immune type B group in both of the training and validation cohorts. AUCs were calculated to examine the predictive value of the immunoscore. As shown in Figure S4c, S4f, S4i and S4j, the immune score had good predictive ability in both cohorts. Additionally, in multivariable models classified by

clinicopathologic characteristics, the salutary effects of immune type A on OS (Figure S5) and DFS (Figure S6) were found to be consistent across all the subgroups (all interaction  $P$  values  $> .05$ ).

According to tumor budding grade and immune type of tumors, we classified patients into four subgroups:  $\text{IS}_A\text{-TB}_{\text{high}}$  (type I),  $\text{IS}_B\text{-TB}_{\text{high}}$  (type II),  $\text{IS}_A\text{-TB}_{\text{low}}$  (type III) and  $\text{IS}_B\text{-TB}_{\text{low}}$  (type IV). In the training cohort, the survival analyses showed that patients with type III tumor had the best OS and DFS, while OS and DFS were the worst for cases with type II tumor (Figure 5(a–b)). Similar results were observed in the validation cohort (Figure 5(c–d)). Multivariable COX



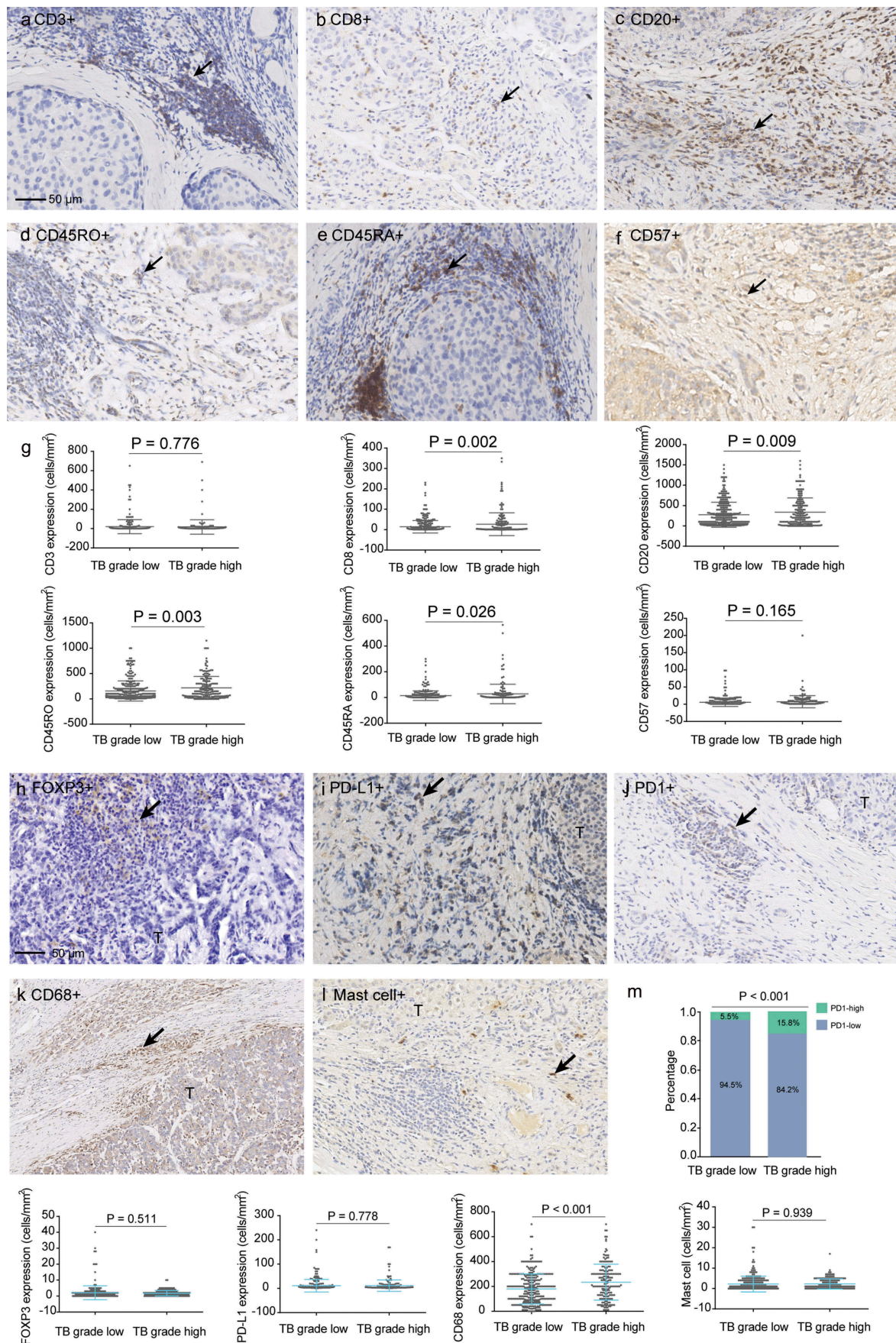


**Figure 4.** Associations of tumor budding with immune cell infiltrations. (a–f) representative images of CD3, CD8, CD20, CD45RO, CD45RA, and CD57. (g) Associations of tumor budding grade with expressions of CD3, CD8, CD20, CD45RO, CD45RA and CD57 in the tumor samples. (h–l), representative images of FOXP3, PD-L1, PD1, CD68 and mast cells. (m) Associations of tumor budding grade with expressions of FOXP3, PD-L1, PD1, CD68 and mast cells.

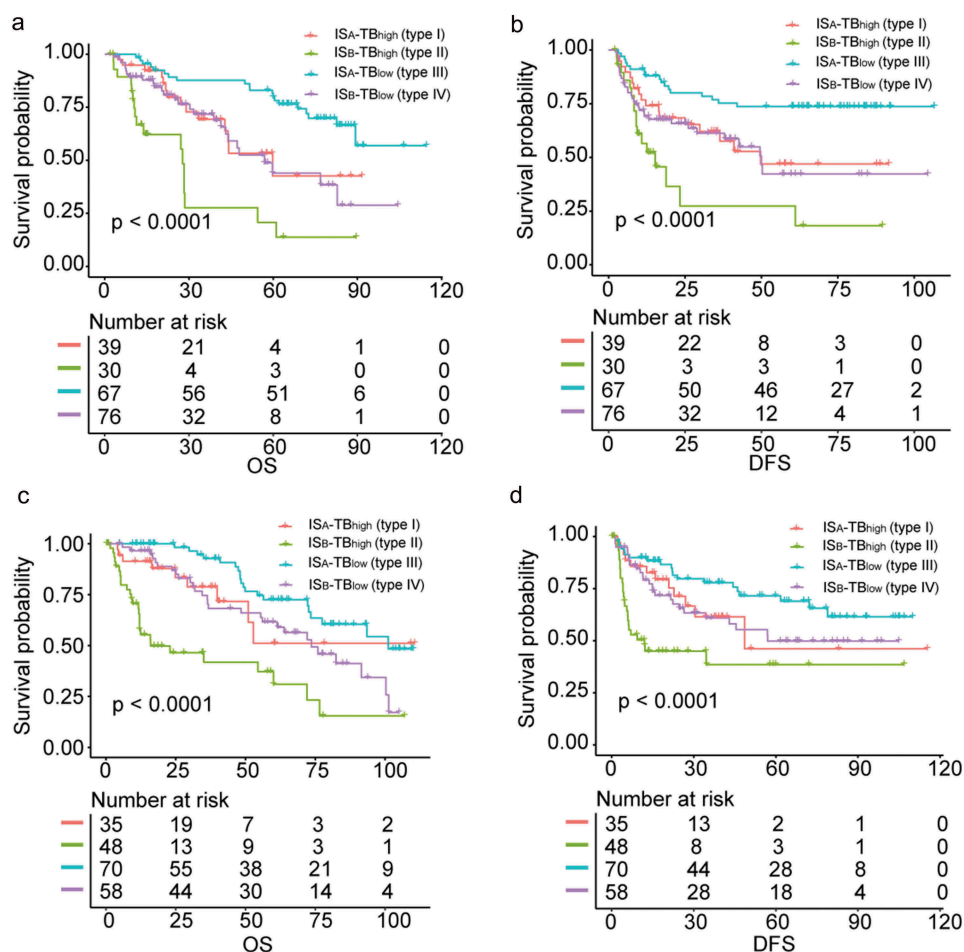


**Figure 5.** Survival analyses comparing the overall and disease-free survival among four HCC subgroups classified by IS-TB type. (a) overall survival in the training cohort. (b) disease-free survival in the training cohort. (c) overall survival in the validation cohort. (d) disease-free survival in the validation cohort.

**Table 2.** Multivariable analysis in the training cohort.

Variables in the final model	HR	95%CI	P
<b>Overall survival</b>			
HBV infection, yes vs. no	1.62	0.83–3.16	0.161
MVI, yes vs. no	2.02	1.28–3.17	0.002
IS-TB type			
Type II vs. type I and IV	3.07	1.83–5.13	< 0.001
Type III vs. type I and IV	0.50	0.29–0.87	0.013
<b>Disease-free survival</b>			
MVI, yes vs. no	2.01	1.42–2.85	< 0.001
AFP level, $\geq 400$ ng/ml vs. < 400 ng/ml	1.56	1.12–2.19	0.009
Tumor differentiation, grade III-IV vs. grade I-II	1.43	1.01–2.03	0.045
IS-TB type			
Type II vs. type I and IV	2.06	1.38–3.07	< 0.001
Type III vs. type I and IV	0.60	0.40–0.91	0.015

HBV, hepatitis b virus; MVI, microvascular invasion; ALBI, albumin-bilirubin; AFP, alpha fetoprotein; HR, hazard ratio; CI, confidence interval.

regression analysis of relevant clinical variables and IS-TB type revealed that IS-TB type was an independent prognostic factor for OS and DFS in the training cohort (Table 2). Given the similar survival of type I and type IV, we grouped the two types together for multivariable analyses.

We developed two nomograms integrating the IS-TB type and clinicopathologic risk variables (Table 2) to predict the probability of 1-, 3- and 5-year DFS (Figure S7(a)) and OS (Figure S7(d)) in cases with HCC. The predictive accuracy (1-, 3-, 5-year AUC) of the nomogram for DFS in the

training and validation cohort is shown in Figure S7(b) and S7c. The C-index for OS and DFS prediction in the training cohort was 0.74 (95% confidence interval, 0.68–0.80) and 0.74 (95% confidence interval, 0.69–0.79), respectively. The C-index for OS and DFS prediction in the validation group was 0.75 (95% confidence interval, 0.70–0.81) and 0.75 (95% confidence interval, 0.70–0.79), respectively. The predictive ability was confirmed in the validation cohort (Figure S7(e–f)). Calibration curves showed that the models performed well when compared to the performance of the ideal models in both cohorts (Figure S8). The nomograms also had better predictive ability in both cohorts in comparison with the TNM (8th) and BCLC staging systems (Figure S9).

### Associations between IS-TB type and molecular alterations

We performed cluster analysis of the data derived from 100 patients who received whole-exome sequencing (Figure S10) from our cohort. We classified patients into four groups based on IS-TB type. A heat-map showing the main pathological, immune and mutational features linked to IS-TB type is provided in Figure 6. Interestingly, associations were observed between molecular mutations and IS-TB type. TP53 mutation



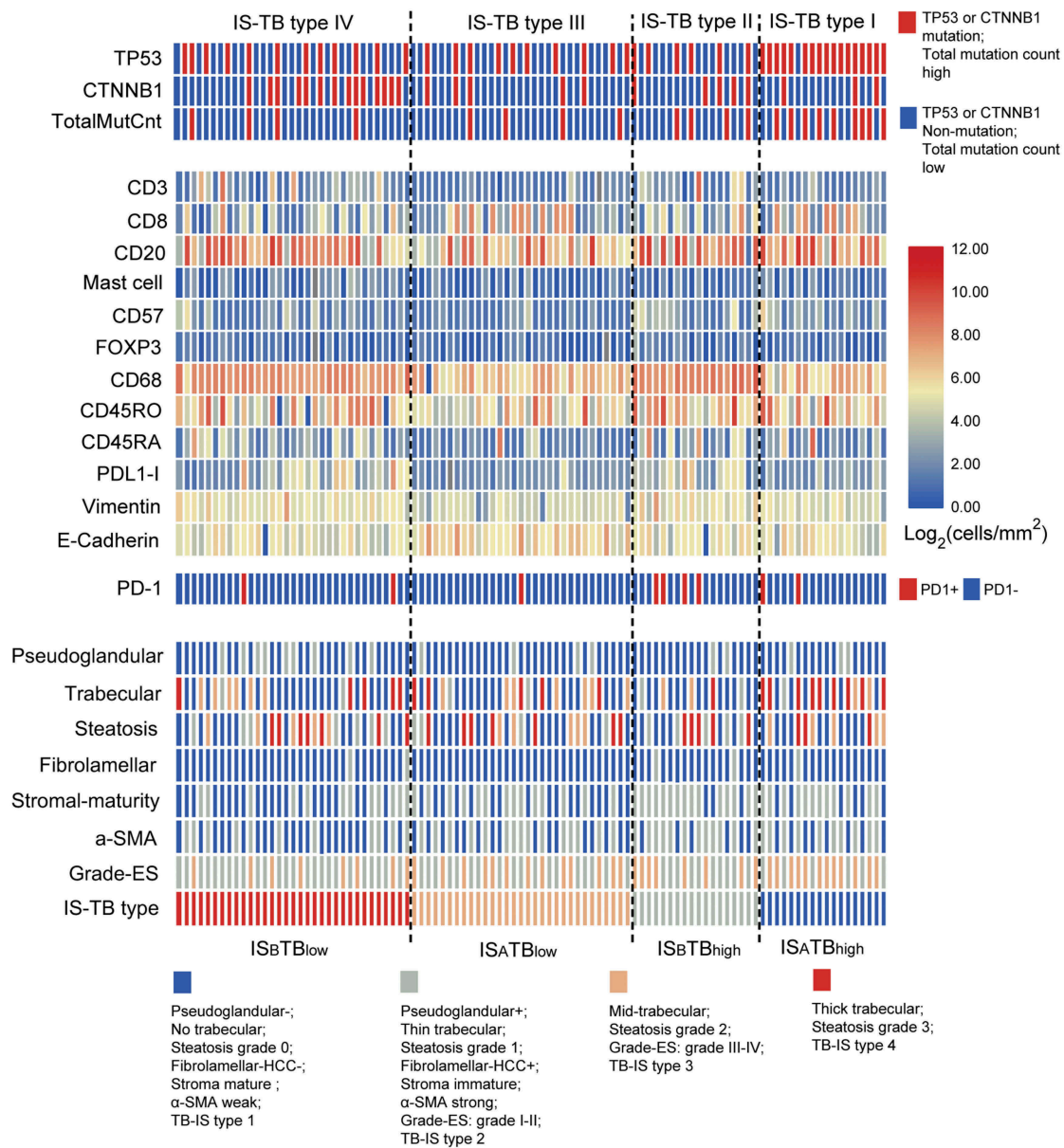


**Figure 6.** Summary of the molecular, immune and pathological characteristics in the 100 patients receiving whole-exome sequencing. Patients were clustered based on IS-TB types.

was more frequent in IS-TB type I (IS<sub>A</sub>TB<sub>high</sub>) patients. In addition, there is a higher incidence of patients in IS-TB type I showing high total mutation count. IS-TB type I also exhibited high level of pseudoglandular pathological pattern, high level of CD8+ immune cell, and low levels of CD68+ and PD-L1+ immune cells. Especially, IS-TB type IV (IS<sub>B</sub>TB<sub>low</sub>) harbored high number of CTNNB1 mutation. Meanwhile, it exhibited high levels of well-differentiated tumor, pseudoglandular pathological pattern, mature stroma and low level of α-SMA expression. As described above, IS-TB type II (IS<sub>B</sub>TB<sub>high</sub>) and III (IS<sub>A</sub>TB<sub>low</sub>) had the worst and best long-term prognosis, respectively. However, both total mutation count and the most frequent mutated molecules showed similar patterns between two groups, which indicated that IS-TB type, not the mutation features, could stratify patients with distinct risks. The immune infiltrate in IS-TB type II was dominated by CD68+ macrophages and PD-L1+ lymphocytes

with low level of CD8 + T cells. In contrast, IS-TB type II exhibited relatively low levels of CD68+ macrophages and PD-L1+ immune cells, while a higher level of CD8 + T cells.

## Discussion

Risk evaluation and treatment allocation for HCC cases are in need of improvement. A growing evidence shows that the TME contributes to tumor differentiation, proliferation, and distant metastasis.<sup>40</sup> In this study, the two promising candidate prognostic indicators involve two different aspects of the TME: tumor budding and the immunoscore. Tumor budding appears to indicate an aggressive phenotype of tumors, while the immune score reflects the diversity of immune response in the TME. The present study reveals relationships linking tumor budding and patient prognosis, pathological features,

and immune cell infiltrations. In addition, according to tumor budding grade and immune type, HCC patients could be classified into distinct subgroups (IS-TB type) related to different prognosis and molecular alterations.

Tumor budding, independent of tumor grade, MVI, and other pathological parameters, was an adverse prognostic factor in HCC. Tumor budding is previously studied in other types of tumor, especially in colorectal cancer.<sup>8</sup> This is the first study demonstrating tumor budding as an adverse prognostic factor in patients with HCC. Moreover, tumor budding was associated with EMT markers and had higher incidences in patients with non-steatotic, non-fibrolamellar-HCC, stromal active (high  $\alpha$ -SMA expression) and immature tumors. A link between tumor budding and EMT makers (E-cadherin and vimentin) confirmed the hypothesis that tumor budding may represent the EMT process. Tumor budding numbers were distinct in specific pathological types and stroma patterns indicated that both of the tumor cell biological behavior and stroma phenotype would impact on the metastatic process of HCC.<sup>31,41</sup>

The role of the immune milieu of HCC as a prognostic feature is also only starting to emerge. Multiple immunosuppressive mechanisms are engaged in HCC.<sup>31,42</sup> In this study, immune score integrated five types of immune cells (CD68+, CD8+, FOXP3+, mast cell, and PD-L1+) in HCC could predict patient survival efficiently (Figure S4). In the present study, we have linked macrophages, mast cells and Tregs to poor DFS and OS, which is consistent with other studies in HCC.<sup>43–45</sup> On the contrary, CD8 + T cells were related to a prolonged DFS and OS. This is also in accordance with previous observations that CD8 + T cells were the main force of anti-tumoral immunity.<sup>31</sup> The interaction and relationship between tumor budding and tumor immune responses are rarely explored. In this study, we have demonstrated that tumor budding was associated with several types of immune cell infiltration in HCC patients, and tumor budding grade was related to both anti- (e.g., CD8 + T cells) and pro-tumor (e.g. CD68+ macrophages) immune responses. Consistently, our IS-TB type based on immune score and tumor budding indicated that a portion of HCC patients had high-grade tumor budding but limited anti-tumor immune responses (IS-TB type II). Consequently, cases within IS-TB type II showed the worst long-term survival. In contrast, cases with low-grade tumor budding and strong immune responses (immune type A) were grouped into IS-TB type III, which had the best OS and DFS. This theory was also supported by the study of Lugli and colleagues.<sup>46</sup> They found that high lymphocyte to tumor budding ratio was a good prognostic factor in patients with colorectal tumor. Lang-Schwarz, et al. also reported that the integration of both TILs and tumor budding could predict long-term prognosis in colorectal cancer.<sup>47</sup> Our results provide a rationale for the pathological evaluation of the TME in addition to the current pathological classifications of HCC.

In this study, we observed that IS-TB type can better define the long-term prognosis of HCC cases, and better identify cases at high risk of recurrence regardless of mutation status. Patients with IS-TB type III and type II had the best and worst survival outcome, respectively. In comparison, in some other tumor types such as melanoma, mutational load was

correlated with the degree of survival benefit.<sup>48</sup> In the present study, nomograms integrating information of IS-TB type, AFP level (DFS), HBV infection (OS), MVI and tumor grade (DFS) were developed, and the models showed better prognostic abilities than BCLC or TNM stages alone in both of the training and validation groups. Consequently, the nomograms provide clinicians with a more reliable tool for better prediction of HCC survival.

IS-TB type was associated with HCC molecular alterations (Figure 6). TP53 (mainly within IS-TB type I) and CTNNB1 (mainly within IS-TB type IV) mutation in HCC dominated two distinct HCC phenotypes, associated with different immune and pathological characteristics. We found that CTNNB1 mutation was associated with impaired anti-tumor immunity (immune type B). Spranger et al. showed that activated  $\beta$ -catenin signaling pathway could defect the anti-tumoral immunity by impairing the recruitment of dendritic cells to the TME.<sup>49</sup> In human metastatic melanoma, researchers also found a relationship between activation of the WNT/ $\beta$ -catenin pathway and absence of a T-cell gene expression landscape.<sup>49,50</sup> In addition, we observed that CTNNB1 mutated tumors were well differentiated, with pseudoglandular pattern, mature stroma, and low  $\alpha$ -SMA (fibroblast activation protein) expression. As reported previously,<sup>41</sup> CTNNB1 mutations activating  $\beta$ -catenin are oncogenic driver mutations related to a specific HCC subtype presented in well-differentiated tumors with pseudoglandular pattern and other specific pathological features. In this study, we revealed the relationship of CTNNB1 mutation and tumor-stromal features in HCC firstly. In addition to CTNNB1, TP53 represented another HCC phenotype in this study. TP53 mutation was poorly differentiated and with thick-trabecular pattern. These observations were also consistent with previous study.<sup>41</sup>

The development of anti-tumoral immunity is believed to be conditioned by the number of tumor neoantigens which represent mutated peptides.<sup>51</sup> Based on this overall hypothesis, we found that patients with immune type A and high-grade tumor budding (IS-TB type I) had the highest incidence of total mutation count. However, we have also observed that a portion of HCC with robust anti-tumor immune responses did not harbor a high mutation count (IS-TB type III), which indicated that gene mutation alone cannot completely explain the anti-tumoral immune responses in HCC.

There were limitations in this study. First, IBTCC method was a standardized assessment method for patients with colorectal cancers, its applicability in HCC should be validated by further studies. Second, we counted immune cells and tumor budding within both the invasive margin and the tumor tissues to reflect a whole landscape of HCC immune cell infiltration. However, the number and types of immune cells and tumor budding in the tumor core and invasive margin may exist distinct significance for tumor treatment and prognostic prediction.

Altogether, we report five major observations: first, we have shown significant relations between tumor budding and patient prognosis; second, tumor budding was associated with specific pathological patterns and immune cell infiltrations in HCC; third, the IS-TB type based on immune score and tumor budding was an independent prognostic factor,

integrating IS-TB type and other clinical parameters could predict patient prognosis efficiently; fourth, IS-TB type was correlated with HCC molecular alterations; fifth, TP53 (mainly corresponds to IS-TB type I) and CTNNB1 (mainly corresponds to IS-TB type IV) mutation in HCC constituted two distinct HCC phenotypes, associated with distinct immune and pathological features. This study can serve as a reference for further researches on the prognostic significance of the interplay between different cell types (e.g., tumor cell and immune cell) within the heterogeneous TME of HCC patients. Our results should be validated in distinct clinical conditions, for instance, in advanced tumors with only biopsy samples.

## Disclosure of Potential Conflicts of Interest

No potential conflicts of interest were disclosed.

## Funding

This work was supported by grants from the National Key Technologies R&D Program [2018YFC1106800]; the Natural Science Foundation of China [81872004, 81800564, 81770615, 81700555 and 81672882]; the Science and Technology Support Program of Sichuan Province [2017SZ0003, 2018SZ0115 and 2017FZ0048]; the Science and Technology Program of Tibet Autonomous Region [XZ201801-GB-02] and the 1.3.5 project for disciplines of excellence, West China Hospital, Sichuan University [ZYJC18008].

## References

- EASL Clinical Practice. Guidelines: management of hepatocellular carcinoma. *J Hepatol.* 2018;69(1):182–236. doi:10.1016/j.jhep.2018.03.019.
- Liu PH, Hsu CY, Hsia CY, Lee YH, Su CW, Huang YH, Lee FY, Lin HC, Huo TI. Prognosis of hepatocellular carcinoma: assessment of eleven staging systems. *J Hepatol.* 2016;64(3):601–608. doi:10.1016/j.jhep.2015.10.029.
- Minagawa M, Ikai I, Matsuyama Y, Yamaoka Y, Makuuchi M. Staging of hepatocellular carcinoma: assessment of the Japanese TNM and AJCC/UICC TNM systems in a cohort of 13,772 patients in Japan. *Ann Surg.* 2007;245(6):909–922. doi:10.1097/01.sla.0000254368.65878.da.
- Cheng CH, Lee CF, Wu TH, Chan KM, Chou HS, Wu TJ, Yu MC, Chen TC, Lee WC, Chen MF. Evaluation of the new AJCC staging system for resectable hepatocellular carcinoma. *World J Surg Oncol.* 2011;9:114. doi:10.1186/1477-7819-9-114.
- Chun YH, Kim SU, Park JY, Kim DY, Han KH, Chon CY, Kim BK, Choi GH, Kim KS, Choi JS, et al. Prognostic value of the 7th edition of the AJCC staging system as a clinical staging system in patients with hepatocellular carcinoma. *Eur J Cancer (Oxford, England: 1990).* 2011;47(17):2568–2575. doi:10.1016/j.ejca.2011.07.002.
- Agopian VG, Harlander-Locke M, Zarrinpar A, Kaldas FM, Farmer DG, Yersiz H, Finn RS, Tong M, Hiatt JR, Busuttil RW. A novel prognostic nomogram accurately predicts hepatocellular carcinoma recurrence after liver transplantation: analysis of 865 consecutive liver transplant recipients. *J Am Coll Surg.* 2015;220(4):416–427. doi:10.1016/j.jamcollsurg.2014.12.025.
- Ryan E, Khaw YL, Creavin B, Geraghty R, Ryan EJ, Gibbons D, Hanly A, Martin ST, O'Connell PR, Winter DC, et al. Tumor budding and PDC grade are stage independent predictors of clinical outcome in mismatch repair deficient colorectal cancer. *Am J Surg Pathol.* 2018;42(1):60–68. doi:10.1097/PAS.0000000000000931.
- van Wyk HC, Park J, Roxburgh C, Horgan P, Foulis A, McMillan DC. The role of tumour budding in predicting survival in patients with primary operable colorectal cancer: a systematic review. *Cancer Treat Rev.* 2015;41(2):151–159. doi:10.1016/j.ctrv.2014.12.007.
- Rogers AC, Winter DC, Heeney A, Gibbons D, Lugli A, Puppa G, Sheahan K. Systematic review and meta-analysis of the impact of tumour budding in colorectal cancer. *Br J Cancer.* 2016;115(7):831–840. doi:10.1038/bjc.2016.274.
- Ueno H, Hase K, Hashiguchi Y, Shimazaki H, Tanaka M, Miyake O, Masaki T, Shimada Y, Kinugasa Y, Mori Y, et al. Site-specific tumor grading system in colorectal cancer: multicenter pathologic review of the value of quantifying poorly differentiated clusters. *Am J Surg Pathol.* 2014;38(2):197–204. doi:10.1097/PAS.000000000000113.
- Lugli A, Kirsch R, Ajioka Y, Bosman F, Cathomas G, Dawson H, El Zimaity H, Flejou JF, Hansen TP, Hartmann A, et al. Recommendations for reporting tumor budding in colorectal cancer based on the International Tumor Budding Consensus Conference (ITBCC) 2016. *Modern Pathol.* 2017;30(9):1299–1311. doi:10.1038/modpathol.2017.46.
- Lugli A, Karamitopoulou E, Zlobec I. Tumour budding: a promising parameter in colorectal cancer. *Br J Cancer.* 2012;106(11):1713–1717. doi:10.1038/bjc.2012.127.
- Fukumoto K, Kikuchi E, Mikami S, Ogihara K, Matsumoto K, Miyajima A, Oya M. Tumor budding, a novel prognostic indicator for predicting stage progression in T1 bladder cancers. *Cancer Sci.* 2016;107(9):1338–1344. doi:10.1111/cas.12990.
- Jesinghaus M, Boxberg M, Konukiewitz B, Slotta-Huspenina J, Schlitter AM, Steiger K, Specht K, Wiczorek K, Warth A, Schmidt T, et al. A novel grading system based on tumor budding and cell nest size is a strong predictor of patient outcome in esophageal squamous cell carcinoma. *Am J Surg Pathol.* 2017;41(8):1112–1120. doi:10.1097/PAS.0000000000000865.
- Jesinghaus M, Bruhl F, Steiger K, Klare P, Reiser M, Scheiter A, Konukiewitz B, Kuhn P, Munch S, Quante M, et al. Cellular dissociation grading based on the parameters tumor budding and cell nest size in pretherapeutic biopsy specimens allows for prognostic patient stratification in esophageal squamous cell carcinoma independent from clinical staging. *Am J Surg Pathol.* 2019;43(5):618–627. doi:10.1097/PAS.0000000000001230.
- Karamitopoulou E, Wartenberg M, Zlobec I, Cibin S, Worni M, Gloor B, Lugli A. Tumour budding in pancreatic cancer revisited: validation of the ITBCC scoring system. *Histopathology.* 2018;73(1):137–146. doi:10.1111/his.13508.
- Karamitopoulou E, Zlobec I, Born D, Kondi-Pafiti A, Lykoudis P, Mellou A, Gennatas K, Gloor B, Lugli A. Tumour budding is a strong and independent prognostic factor in pancreatic cancer. *Eur J Cancer (Oxford, England: 1990).* 2013;49(5):1032–1039. doi:10.1016/j.ejca.2012.10.022.
- Wartenberg M, Cibin S, Zlobec I, Vassella E, Eppenberger-Castori S, Terracciano L, Eichmann MD, Worni M. Integrated genomic and immunophenotypic classification of pancreatic cancer reveals three distinct subtypes with prognostic/predictive significance. *Clin Cancer Res.* 2018;24(18):4444–4454. doi:10.1158/1078-0432.CCR-17-3401.
- Kemi N, Eskuri M, Ikalainen J, Karttunen TJ, Kauppila JH. Tumor budding and prognosis in gastric adenocarcinoma. *Am J Surg Pathol.* 2019;43(2):229–234. doi:10.1097/PAS.0000000000001181.
- Yamada N, Sugai T, Eizuka M, Tsuchida K, Sugimoto R, Mue Y, Suzuki M, Osakabe M, Uesugi N, Ishida K, et al. Tumor budding at the invasive front of colorectal cancer may not be associated with the epithelial-mesenchymal transition. *Hum Pathol.* 2017;60:151–159. doi:10.1016/j.humpath.2016.10.007.
- Wang C, Huang H, Huang Z, Wang A, Chen X, Huang L, Zhou X, Liu X. Tumor budding correlates with poor prognosis and epithelial-mesenchymal transition in tongue squamous cell carcinoma. *J Oral Pathol Med.* 2011;40(7):545–551. doi:10.1111/j.1600-0714.2011.01041.x.
- Karamitopoulou E, Lugli A, Panayiotides I, Karakitsos P, Peros G, Rallis G, Patsouris ES, Terracciano L, Zlobec I. Systematic assessment of protein phenotypes characterizing high-grade tumour budding in mismatch repair-proficient colorectal cancer. *Histopathology.* 2010;57(2):233–243. doi:10.1111/j.1365-2559.2010.03615.x.



23. Miksch RC, Schoenberg MB. Prognostic impact of tumor-infiltrating lymphocytes and neutrophils on survival of patients with upfront resection of pancreatic cancer. *Cancers (Basel)*. 2019 Jan 3;11(1). pii: E39. doi: [10.3390/cancers11010039](https://doi.org/10.3390/cancers11010039).
24. Mlecnik B, Bindea G, Angell HK, Maby P, Angelova M, Tougeron D, Church SE, Lafontaine L, Fischer M, Fredriksen T, et al. Integrative analyses of colorectal cancer show immunoscore is a stronger predictor of patient survival than microsatellite instability. *Immunity*. 2016;44(3):698–711. doi:[10.1016/j.immuni.2016.02.025](https://doi.org/10.1016/j.immuni.2016.02.025).
25. Bense RD, Sotiriou C, Piccart-Gebhart MJ, Haanen J, van Vugt M, de Vries EGE, Schroder CP, Fehrmann RSN. Relevance of tumor-infiltrating immune cell composition and functionality for disease outcome in breast cancer. *J Natl Cancer Inst*. 2017;109(1). doi:[10.1093/jnci/djx007](https://doi.org/10.1093/jnci/djx007).
26. Mlecnik B, Van den Eynde M, Bindea G, Church SE, Vasaturo A, Fredriksen T, Lafontaine L, Haicheur N, Marliot F, Debetancourt D, et al. Comprehensive intrametastatic immune quantification and major impact of immunoscore on survival. *J Natl Cancer Inst*. 2018;110(1). doi:[10.1093/jnci/djx216](https://doi.org/10.1093/jnci/djx216).
27. Sideras K, Biermann K, Verheij J, Takkenberg BR, Mancham S, Hansen BE, Schutz HM, de Man RA, Sprengers D, Buschow SI, et al. PD-L1, galectin-9 and CD8(+) tumor-infiltrating lymphocytes are associated with survival in hepatocellular carcinoma. *Oncoimmunology*. 2017;6(2):e1273309. doi:[10.1080/2162402X.2016.1273309](https://doi.org/10.1080/2162402X.2016.1273309).
28. Calderaro J, Petitprez F, Becht E, Laurent A, Hirsch TZ, Rousseau B, Luciani A, Amaddeo G, Derman J, Charpy C, et al. Intra-tumoral tertiary lymphoid structures are associated with a low risk of early recurrence of hepatocellular carcinoma. *J Hepatol*. 2019;70(1):58–65. doi:[10.1016/j.jhep.2018.09.003](https://doi.org/10.1016/j.jhep.2018.09.003).
29. Gabrielson A, Wu Y, Wang H, Jiang J, Kallakury B, Gatalica Z, Reddy S, Kleiner D, Fishbein T, Johnson L, et al. Intratumoral CD3 and CD8 T-cell densities associated with relapse-free survival in HCC. *Cancer Immunol Res*. 2016;4(5):419–430. doi:[10.1158/2326-6066.CIR-15-0110](https://doi.org/10.1158/2326-6066.CIR-15-0110).
30. Hu G, Wang S. Tumor-infiltrating CD45RO(+) memory T lymphocytes predict favorable clinical outcome in solid tumors. *Sci Rep*. 2017;7(1):10376. doi:[10.1038/s41598-017-11122-2](https://doi.org/10.1038/s41598-017-11122-2).
31. Kurebayashi Y, Ojima H, Tsujikawa H, Kubota N, Maehara J, Abe Y, Kitago M, Shinoda M, Kitagawa Y, Sakamoto M. Landscape of immune microenvironment in hepatocellular carcinoma and its additional impact on histological and molecular classification. *Hepatol (Baltimore, Md)*. 2018;68(3):1025–1041. doi:[10.1002/hep.29904](https://doi.org/10.1002/hep.29904).
32. Jiang Y, Zhang Q, Hu Y, Li T, Yu J, Zhao L, Ye G, Deng H, Mou T, Cai S, et al. ImmunoScore signature: a prognostic and predictive tool in gastric cancer. *Ann Surg*. 2018;267(3):504–513. doi:[10.1097/SLA.0000000000002116](https://doi.org/10.1097/SLA.0000000000002116).
33. Li W, Li L, Minigalin D, Wu H. Anatomic mesohepatectomy versus extended hepatectomy for patients with centrally located hepatocellular carcinoma. *HPB*. 2018;20(6):530–537. doi:[10.1016/j.hpb.2017.11.012](https://doi.org/10.1016/j.hpb.2017.11.012).
34. Johnson PJ, Berhane S, Kagebayashi C, Satomura S, Teng M, Reeves HL, O'Beirne J, Fox R, Skowronska A, Palmer D, et al. Assessment of liver function in patients with hepatocellular carcinoma: a new evidence-based approach-the ALBI grade. *J Clin Oncol*. 2015;33(6):550–558. doi:[10.1200/JCO.2014.57.9151](https://doi.org/10.1200/JCO.2014.57.9151).
35. Ueno H, Jones AM, Wilkinson KH, Jass JR, Talbot IC. Histological categorisation of fibrotic cancer stroma in advanced rectal cancer. *Gut*. 2004;53(4):581–586. doi:[10.1136/gut.2003.028365](https://doi.org/10.1136/gut.2003.028365).
36. Graham RP, Vierkant RA, Tillmans LS, Wang AH, Laird PW, Weisenberger DJ, Lynch CF, French AJ, Slager SL, Raissian Y, et al. Tumor budding in colorectal carcinoma: confirmation of prognostic significance and histologic cutoff in a population-based cohort. *Am J Surg Pathol*. 2015;39(10):1340–1346. doi:[10.1097/PAS.0000000000000504](https://doi.org/10.1097/PAS.0000000000000504).
37. Fu H, Zhu Y, Wang Y, Liu Z, Zhang J, Xie H. Identification and validation of stromal immunotype predict survival and benefit from adjuvant chemotherapy in patients with muscle-invasive bladder cancer. *Clin Cancer Res*. 2018;24(13):3069–3078.
38. Jiang Y, Xie J, Han Z, Liu W, Xi S, Huang L, Huang W, Lin T, Zhao L, Hu Y, et al. Immunomarker support vector machine classifier for prediction of gastric cancer survival and adjuvant chemotherapeutic benefit. *Clin Cancer Res*. 2018;24(22):5574–5584. doi:[10.1158/1078-0432.CCR-18-0848](https://doi.org/10.1158/1078-0432.CCR-18-0848).
39. Wolowich WR, Casavant MJ, Ekins BR. Phenylpropanolamine and hemorrhagic stroke. *N Engl J Med*. 2001;344(14):1094–1095. doi:[10.1056/NEJM200104053441411](https://doi.org/10.1056/NEJM200104053441411).
40. Church SE, Galon J. Tumor microenvironment and immunotherapy: the whole picture is better than a glimpse. *Immunity*. 2015;43(4):631–633. doi:[10.1016/j.immuni.2015.10.004](https://doi.org/10.1016/j.immuni.2015.10.004).
41. Calderaro J, Couchy G, Imbeaud S, Amaddeo G, Letouze E, Blanc JF, Laurent C, Hajji Y, Azoulay D, Bioulac-Sage P, et al. Histological subtypes of hepatocellular carcinoma are related to gene mutations and molecular tumour classification. *J Hepatol*. 2017;67(4):727–738. doi:[10.1016/j.jhep.2017.05.014](https://doi.org/10.1016/j.jhep.2017.05.014).
42. Sia D, Jiao Y, Martinez-Quetglas I, Kuchuk O, Villacorta-Martin C, Castro de Moura M, Putra J, Camprecios G, Bassaganyas L, Akers N, et al. Identification of an immune-specific class of hepatocellular carcinoma, based on molecular features. *Gastroenterology*. 2017;153(3):812–826. doi:[10.1053/j.gastro.2017.06.007](https://doi.org/10.1053/j.gastro.2017.06.007).
43. Hu G, Wang S, Cheng P. Tumor-infiltrating tryptase(+) mast cells predict unfavorable clinical outcome in solid tumors. *Int J Cancer*. 2018;142(4):813–821. doi:[10.1002/ijc.31099](https://doi.org/10.1002/ijc.31099).
44. Miao L, Liu Q, Lin CM, Luo C, Wang Y, Liu L, Yin W, Hu S, Kim WY, Huang L. Targeting tumor-associated fibroblasts for therapeutic delivery in desmoplastic tumors. *Cancer Res*. 2017;77(3):719–731. doi:[10.1158/0008-5472.CAN-16-0866](https://doi.org/10.1158/0008-5472.CAN-16-0866).
45. Lim CJ, Lee YH, Pan L, Lai L, Chua C, Wasser M, Lim TKH, Yeong J, Toh HC, Lee SY, et al. Multidimensional analyses reveal distinct immune microenvironment in hepatitis B virus-related hepatocellular carcinoma. *Gut*. 2019;68(5):916–927. doi:[10.1136/gutjnl-2018-316510](https://doi.org/10.1136/gutjnl-2018-316510).
46. Lugli A, Karamitopoulou E, Panayiotides I, Karakitsos P, Rallis G, Peros G, Iezzi G, Spagnoli G, Bihl M, Terracciano L, et al. CD8+ lymphocytes/tumour-budding index: an independent prognostic factor representing a 'pro-/anti-tumour' approach to tumour host interaction in colorectal cancer. *Br J Cancer*. 2009;101(8):1382–1392. doi:[10.1038/sj.bjc.6605318](https://doi.org/10.1038/sj.bjc.6605318).
47. Lang-Schwarz C, Melcher B, Haumaier F, Lang-Schwarz K, Rupprecht T, Vieth M, Sterlacci W. Budding and tumor-infiltrating lymphocytes - combination of both parameters predicts survival in colorectal cancer and leads to new prognostic subgroups. *Hum Pathol*. 2018;79:160–167. doi:[10.1016/j.humpath.2018.05.010](https://doi.org/10.1016/j.humpath.2018.05.010).
48. Lauss M, Donia M, Harbst K, Andersen R, Mitra S, Rosengren F, Salim M, Vallon-Christersson J. Mutational and putative neoantigen load predict clinical benefit of adoptive T cell therapy in melanoma. *Nat Commun*. 2017;8(1):1738.
49. Spranger S, Bao R, Gajewski TF. Melanoma-intrinsic beta-catenin signalling prevents anti-tumour immunity. *Nature*. 2015;523(7559):231–235. doi:[10.1038/nature14404](https://doi.org/10.1038/nature14404).
50. Spranger S, Gajewski TF. Tumor-intrinsic oncogene pathways mediating immune avoidance. *Oncoimmunology*. 2016;5(3):e1086862. doi:[10.1080/2162402X.2015.1086862](https://doi.org/10.1080/2162402X.2015.1086862).
51. Knudsen ES, Vail P, Balaji U, Ngo H, Botros IW, Makarov V, Riaz N, Balachandran V, Leach S, Thompson DM, et al. Stratification of pancreatic ductal adenocarcinoma: combinatorial genetic, stromal, and immunologic markers. *Clin Cancer Res*. 2017;23(15):4429–4440. doi:[10.1158/1078-0432.CCR-17-0162](https://doi.org/10.1158/1078-0432.CCR-17-0162).